



On the evolution of substrate's residual stress during cold spray process: A parametric study



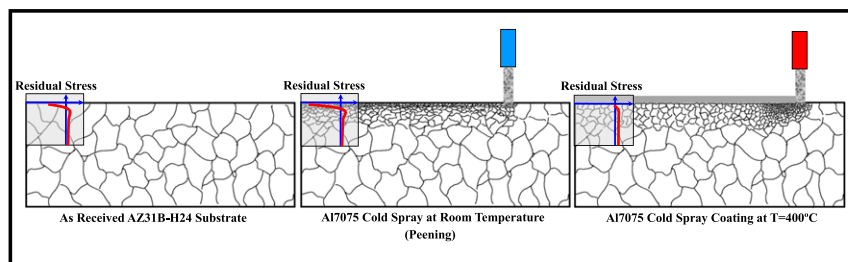
Bahareh Marzbanrad, Hamid Jahed *, Ehsan Toyserkani

Mechanical and Mechatronics Engineering Department, University of Waterloo, Canada

HIGHLIGHTS

- In situ strain/temperature measurement using FBG sensors during cold spray coating of Al7075 particles on AZ31B-H24.
- Statistical model was developed to examine the impact of processing parameters and their interactions on residual stress
- Gas temperature had the most, and gas pressure and the nozzle speed interaction had the least significant impact.
- Substrate grain size, recrystallization, and growth at the interface were a function of the absorbed thermal energy

GRAPHICAL ABSTRACT



ARTICLE INFO

Article history:

Received 1 September 2017

Received in revised form 10 October 2017

Accepted 22 October 2017

Available online 24 October 2017

Keywords:

Cold spray
Magnesium alloys
Aluminum powder
Residual stress
Grain refinement
Fatigue failure

ABSTRACT

A comprehensive study was undertaken to determine the effects of carrier gas temperature, pressure, and nozzle speed on the residual stresses induced by cold spray coating of aluminum 7075 powder onto AZ31B-H24 magnesium substrate. Embedded Fiber Bragg Grating sensors and thermocouples were employed for simultaneous in-situ measurements of strain and temperature during cold spray process. A statistical model was then developed based on the significance and interactions of the cold spray parameters on the residual stress field. This model demonstrated that the induced temperature is the most significant parameter to the final formation of residual stress. It is also shown that the peening effect plus the temperature resulted from the cold spray yields to the dynamic recrystallization of the substrate near the surface, and generates nano-size grains at the interface. This research validates that the final size of the refined grains and the level of induced residual stress depend heavily on the process' thermal energy.

© 2017 Elsevier Ltd. All rights reserved.

1. Introduction

Developing effective approaches to extending the life of aging structural materials is a major challenge, particularly for load-bearing components. Since majority of structural failure is attributable to fatigue, research focused on the enhancement of fatigue strength in structural materials has become significant [1]. For this purpose, inducing

beneficial residual stresses at critical locations, where fatigue cracks nucleate, is shown to be a successful approach to postponing the fatigue crack failure of mechanical components during service [2,3]. Moreover, strengthening the material surface with the coating of high fatigue resistance material is a technique for increasing the life of a low fatigue strength material [4]. "Cold Gas Dynamic Spray" technology, a solid state coating process, creates both mentioned benefits [5]. This coating method can be used to deposit micron-sized metal particles that have been accelerated to a high velocity (300–1200 m/s) onto a material's surface via a de Laval nozzle [6]. The particles and substrate are severely

* Corresponding author.

E-mail address: hjahedmo@uwaterloo.ca (H. Jahed).

deformed upon impact, resulting in mechanical/metallurgical bonding between the substrate and coating because of adiabatic shear instability [7]. On the other hand, the surface hardening treatment result of a peening effect can induce compressive residual stress as well as grain refinement in the coated material. Up to now, numerous studies involving cold spray technique have shed light on the bonding mechanism, coating quality, and applications toward corrosion and wear resistance. However, in spite of the important role of cold spray in improving the fatigue life of materials [8–10], this topic has been addressed in only a few cases, with some contradictory results regarding the effectiveness of cold spray in enhancing fatigue life [11,12].

To date, a few studies have attempted to evaluate the impact of the cold spray on the fatigue behaviour of materials through consideration of four main factors: 1) the properties and quality of a coating material [12–14], 2) bond strength [8,11,15], 3) surface roughness [16] and, 4) residual stress induced by the coating process [17,18]. The first three certainly have essential roles in enhancing the fatigue performance of coated samples, while detrimental residual stress distribution can remove all benefits and decrease fatigue strength [8,11]. Despite reports on minimal effect of residual stress on the fatigue life of coated materials [18,19], research on controlling residual stress distribution in both coating and substrate are necessary and critical [11,20]. However, there is little published data addressing the formation and distribution of residual stress induced during cold spray process.

Compressive residual stress may be generated in a substrate and/or coating due to high impact energy associated with the particles' mass and velocity. A particle velocity that is high enough to achieve the best quality of coating without interface delamination is provided through tuning the effective parameters, pressure and temperature, of the carrier gas [21–23]. However, there have been mixed findings about the carrier gas pressure and/or the temperature contribution to the final coating characteristic as well as to induced residual stress and fatigue performance of coated samples [8,10,19]. Cavaliere et al. [10] investigated the role of processing parameters on the residual stress and fatigue performance of coated samples: Al7075/Al7075, Al2024/Al7075, and Al2024/AZ91 coating/substrates. They found that with increasing the gas pressure and decreasing gas temperature, the compressive residual stress at the interface near the substrate was increased for coated Al alloys on the Al7075. However, gas pressure changes had more noticeable beneficial effects on the variation of residual stress of AZ91 coated sample compare to the other ones [10]. They further reported that in both Al/Al and Al/Mg cases the coating lead to increase in fatigue life with surface residual stresses playing a major role. Luzin et al. [19] studied the residual stress profiles of Al/Cu as coating and substrate materials at different conditions. They revealed that the residual stresses were strongly depending on the plastic deformation due to the impact velocity; whereas thermal effects were not playing an important role in changing the residual stress profile. Ghelichi et al. [8] studied Al/Al cold spray coating and observed that despite Al7075 higher hardness as compared to pure Al, the residual stress induced by Al7075 powder were lower than the ones induced by pure Al. They attributed this to the higher temperature in Al7075 coating. The difference between the studies is strongly related to the material property of coatings and substrates. Moreover, it is reported that the strength of the substrate and coating material [24,25] as well as the substrate temperature [26] affect the residual stress of the coating and substrate. Hence, the effect of cold spray coating parameters on the residual stress and, as a consequence, the fatigue life of coated sample, can be accurately explained when the substrate and coating materials are both considered.

Due to the high demand for reducing greenhouse gas emissions, lightweighting of transportation vehicles have recently received major attention [27]. In particular, the application of Mg alloys, as the lightest commercially available structural metals with superior properties (e.g., a high strength-to-weight ratio), for use in auto and aerospace industries has risen dramatically [28]. However, low corrosion, wear and fatigue resistances have restricted their widespread use in structural

applications, particularly in load-bearing components [29,30]. Based on the nature of cold spraying, cold deposition of a fatigue-resistance metal powder on magnesium substrate can be an ideal solution to boost the fatigue performance of the Mg alloy [9,10,13,31]. However, the induced residual stress of Mg substrates after cold spraying has been reported to range from compressive to tensile, corresponding to processing parameters and coating materials [10,18,19]. On the other hand, since high thermal sensitivity and low-strength of magnesium alloys are more susceptible to residual stress changes, a comprehensive study of the residual stress evolution during cold spraying of these materials is of more interest in identifying the role of different coating parameters in the formation of residual stresses. Determination of the parameter most significant to optimal coating conditions will lead to increased beneficial residual stress and improved Mg alloy microstructure, thereby enhancing fatigue life.

To better understand the interaction between thermal and mechanical strains induced during cold spray coating, we present the in-situ thermo-mechanical behaviour of Mg alloy substrate undergoing cold spraying. Embedded Fiber Bragg Grating (FBG) sensors and thermocouples are simultaneously employed to monitor strain and temperature changes during the cold spray process. The effect of cold spraying on the substrate's microstructure and interface is investigated under various carrier gas temperatures and pressures. A set of experiments has been designed to study the role of carrier gas pressure, temperature, and nozzle travelling speed on a substrate's residual stress. The residual stresses of as-received and cold spray-coated Mg alloy substrates are measured by X-ray diffraction and hole drilling methods. The effect of coating parameters and their interactions on residual stress are statistically analyzed to identify the most significant parameter.

2. Materials and methods

2.1. Material characterization

In this study, for in-situ strain and temperature observation, 4 mm thick AZ31B-H24 Mg alloy sheets were used as the substrate. The chemical composition of the substrate is reported in Table 1. The dimensions and shape of the samples are shown in Fig. 1a and b, respectively. Where applicable, stress relief heat treatment (260 °C/15 min) was carried out on the as-received sheets based on the ASM-recommended procedure [32] to remove any manufacturing related residual stresses. In addition to examining different coating processing parameters on measured residual stress, 12 rectangular pieces of as-received AZ31B-H24 samples (50 × 30 × 3.16 mm) were prepared.

Spherical-shape commercial Al7075 powder (supplied by Centerline Ltd., Windsor, Canada) was the material deposited in the experiments. The SEM image of particles and particle size distribution with a mean value of 23 µm (measured by Retsch Technology, Camsizer XT) is depicted in Fig. 2a and b, respectively. Table 1 lists the chemical composition of the Al7075 powder.

2.2. In-situ strain and temperature measurement

FBG sensors are a class of optical sensors made of hair-thin filaments of fused silica that are able to detect and quantify external stimuli, such as load and temperature, by reflecting wavelength changes [34,35]. Strain evolution can be calculated through a simple equation that considers wavelength changes. The capacity of FBG sensors to measure mechanical (at a constant temperature) or thermo-mechanical strain locally with respect to changes in wavelength has been studied extensively, and shows high accuracy and good agreement with alternative measurement methods [36,37].

Corning SMF-28 FBG sensors with polyimide coating and a reflectivity of 90% were employed for in-situ measurements of strain. The FBG initial wavelength was 1560 nm and the grating length was 10 mm. The sensor's polyimide protective layer was removed from the grating

by dipping the sensor into hot sulfuric acid (98%) for 20 min followed by rinsing with deionized water [36].

The relationship between the wavelength shifts, strain, and temperature changes is specified according to the following equations:

$$\varepsilon = \frac{1}{K} \left(\frac{\Delta\lambda}{\lambda_0} - \alpha_\delta \times \Delta T \right) \quad (1)$$

$$\varepsilon = \varepsilon_m + \varepsilon_T \quad (2)$$

$$\varepsilon_T = \alpha_{sp} \times \Delta T \quad (3)$$

$$\alpha_\delta = \frac{\delta n}{\delta T} \quad (4)$$

where, $\Delta\lambda$ is the wavelength shift, λ_0 is the base wavelength at test start, k is the gauge factor, ε is the total strain caused by force (ε_m) and temperature (ε_T), α_δ is defined by the change of the refractive index with temperature, α_{sp} is the expansion coefficient of the sample (1/K), and ΔT is the temperature change (K). For measuring temperature, a type K thermocouple (300 μm wires) was attached to each sample in such way that it would be able to detect the substrate surface temperature exactly.

Experiments and numerical simulations have shown that during the coating process, stress in a substrate is faded as it approaches 1 mm depth [18,19,31,38]. Therefore, the depth and alignment of the grating of FBG sensor as well as thermocouple were selected carefully to ensure that the maximum strain and temperature changes at and under the substrate surface could be observed during the cold spray coating. Stress-relieved AZ31B-H24 samples were prepared with 90° and 45° aligned 700 μm diameter holes for embedding the FBG sensors, and with a 1 mm diameter hole for the thermocouple (Fig. 1b and c). Then, the sensors and thermocouple were embedded in the holes and adhered by a thin layer of thermal epoxy (353ND EPO-TEK) that was cured at 150 °C [39].

2.3. Cold-spray process

A commercial Supersonic Spray Technologies (SST) Series P Cold Spray System, manufactured by Centerline, Windsor, Canada, was used to coat the as-received samples. In this process, Al7075 powders are accelerated through a converging-diverging de Laval UltiLife TM nozzle to supersonic velocities in a low-pressure system. Table 2 lists the typical processing parameters required for high coating quality. Sample thicknesses were between 300–350 μm , with a high hardness of 139.6 ± 19.4 HV.

2.4. Microstructural analysis

Microstructural analysis was performed using transmission electron microscopy (TEM, JEOL-2010F) and scanning electron microscope (SEM, model: Zeiss Leo UltraPlus FESEMs) equipped with an Oxford energy-dispersive X-ray spectroscope. X-ray spectroscopy determined the chemical composition and surface coverage of the coated surfaces. Treated samples were cross-sectioned in the plane perpendicular to the rolling directions, mounted, polished with a series of graded abrasive papers from ~400 to 1200 grit, followed by fine polishing using

diamond paste from 6 μm to 0.1 μm on Leco paper. Samples were then etched for 10 s in a reagent composed of 35 mL ethanol, 5 mL acetic acid, 2.1 g picric acid and 5 mL water to reveal the grain structure of the Mg alloy samples.

2.5. Residual stress measurement

The hole-drilling and X-ray diffraction methods were used to measure the induced residual stress in the coating and substrate samples. A hole-drilling machine (Sint Technology, Restan MTS-3000) was used to evaluate the distribution of residual stresses through the depth of coated samples by measuring the relaxation strain. For this, conventional HBM three-element strain gauge rosettes were installed on the samples surface in the inspected area. The equipment's air turbine incrementally drilled a 2 mm diameter shallow hole in the middle of the strain gauge rosette, at a speed of 400,000 RPM. The relieved strains were measured through the strain gauge rosette in three different directions. The measured incremental strain data were used to calculate the stress gradient through the depth of the sample by using the integral method [40]. This method is capable of calculating residual stresses corresponding to a highly non-uniform residual stress distribution up to 1 mm depth. In addition, a Bruker D8-Discover equipped with a VÄNTAC-500 area detector with a radius of 135 mm, using Cu-K α radiation at 40 kV and 40 mA, was used for X-ray residual stress measurements. During the measurement, the incident beam and the detector were placed at a fixed 20 angle of 99.22°. The collimator size was 1.0 mm. The sample was mounted on the motorized stage, which was oscillated at amplitudes of 1.5 mm and 2.5 mm at speeds of 3.5 mm/s and 5.5 mm/s for the X and Y axes, respectively. The samples were tilted between 0° and 50° with a step of 25° considered as the Ψ -scan, while the sample rotation known as ϕ -scan was between 0° and 360° with a step size of 45°. The sample was scanned for 60 s at each orientation. The Debye-Scherrer diffraction rings were collected using the area detector in a two-dimensional diffraction image. The complete residual stresses were then calculated using Leptos software in average depth of 50–100 μm corresponding to the penetration coefficient of magnesium alloys [41].

3. Results and discussion

3.1. In-situ strain and temperature monitoring

In-situ monitoring of mechanical and thermal strain was implemented during cold-spray coating deposition process through the FBG sensor embedded in the Mg alloy substrate. The response of the FBG sensor to extension or contraction of the gratings due to thermal and/or mechanical loads is a linear change in the wavelength [36,42]. Fig. 3 shows some critical spectrums obtained at different nozzle positions during cold spraying, and schematically illustrates the relative positions of the nozzle and sensor. The response of the sensor after the embedding process but before coating is depicted in Fig. 3a. The spectrum of the sensor was asymmetric because of the non-uniform strain along the grating. In this case, the spectrum is expanded from the right side, emphasizing an initial elastic strain accumulation close to the substrate surface. When the nozzle approached the sensor (Fig. 3b), pick broadening and shifting to the right of the spectrum happened concurrently. In this condition, thermal strain due to the carrier gas temperature caused

Table 1

Chemical compositions of AZ31B-H24 magnesium alloy [33] and Al7075 coating powder.

Materials	Aluminum (Al)	Zinc (Zn)	Manganese (Mn)	Iron (Fe)	Nickel (Ni)	Silicon (Si)	Copper (Cu)	Chromium (Cr)	Magnesium (Mg)	Other elements
AZ31B-H24	2.5–3.5	0.60–1.40	0.2 Min	0.005 Max	0.005 Max	0.10 Max	0.05 Max	–	Bal.	–
Al7075	90	5.2	–	0.35	0.005	–	1.55	0.25	2.35	0.3

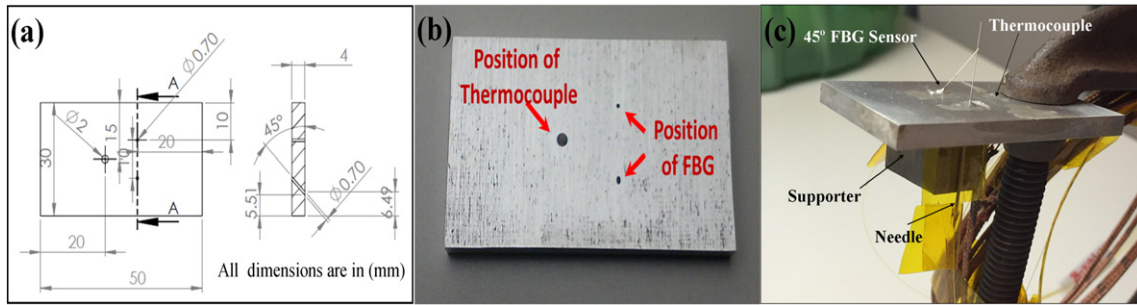


Fig. 1. a) Drawing and geometry of AZ31B-H24 samples; b) position of thermocouple and FBG sensors; c) test sample setup for embedded sensors and thermocouple.

the shifting and broadening of the spectrum. When the distance between the nozzle and sensor is decreased, more stretching and shifting of the spectrum is expected. However, by placing the nozzle exactly above the sensor (see schematic Fig. 3c) the temperature is higher and as a consequence more peak shift and widening would be predicted. However, peak narrowing was observed, although the peak still showed more transition to the right (Fig. 3c). This change of spectrum shape illuminates a significant compressive strain induced by peening and severe plastic deformation during deposition decreasing the effect of thermal expansion. This observation clarified the contrast between peening effect and increasing temperature. After passing the nozzle (Fig. 3d), the peak became broader and transmitted further to the right than before; thus, signs of compressive strain cannot be detected. This is evidence that the induced compressive stress of the substrate can be relieved in a few seconds. Fig. 3e shows the spectrum changes after the cold spraying and the Mg alloy sample reached room temperature. The shape of the spectrum has become narrower; however, the peak has shifted to the right as compared to the first recordings (Fig. 3a). Significant wavelength change after cold spray coating (equivalent to 0.06% tensile strain) highlighted the effect of temperature arising from carrier gas and adiabatic shear deformation as an important factor on the strain evolution during the cold spray process. It is of note that the stress relief process releases the residual elastic energy of the material—in this case not only the compressive stress due to peening was relieved, but also tensile residual strain was resulted in the substrate. This can be explained by considering the thermal mismatch of the Al7075 coating and the AZ31B-H24 substrate. This mismatched strain created tensile residual strain during the cooling process (after the coating was completed). Variation in the residual stress remaining in the system, alternating from compressive to tensile, was also reported in the case of copper deposition on steel via analytical and numerical modelling [43].

In addition to in-situ FBG measurements, simultaneously the temperature at the substrate surface during the cold spray deposition was measured by embedding a thermocouple in the sample. Fig. 4 depicts

the temperature gradient of the substrate sample during a single pass coating. When the nozzle was directly above the thermocouple, the thermal conductivity attributable to the carrier gas temperature in addition to the impact temperature raised the substrate surface temperature to 330 °C. In-situ temperature measurements also revealed that the interface experienced a temperature higher than 260 °C for 46 s. It is well known that increasing the temperature of a metallic crystalline material may cause annealing, which includes recovery, recrystallization and grain growth processes. These processes are both time and temperature dependent. Recovery happens at a lower temperature than the other processes and involves the realignment of dislocations leading to a significant decrease in dislocation density and, as a consequence, reduction of the residual stress even though the crystal structure of the sample is not changed. Recrystallization and grain growth are diffusional processes that require more thermal energy. The annealing process of AZ31B-H24 takes only 20 s at 260 °C [44]. This fact, along with the measured temperature during coating (Fig. 4), can explain the in-situ strain observation reported in Fig. 3. The high velocity Al7075 powder had sufficient energy to deform the substrate and induce compressive residual stress within it. However, the temperature of the carrier gas accompanied by a rapid temperature rise due to adiabatic shear deformation increased the substrate temperature in a way that activated the temperature-dependent mechanisms and released the residual stress.

3.2. Microstructure of the interface

The microstructure of coated samples with the high nozzle velocity ($V = 10$ mm/s) is investigated by TEM. Fig. 5a demonstrates three distinct zones that are visible in the bright field image. A continuous layer of ~200–300 nm is clearly noticeable between the coating and substrate. Grain refinement was observed adjacent to the interface of the substrate. The dark field image (Fig. 5b) shows that the bright spots obtained near the interface are refined grains of ~200 nm. Fig. 5c shows the magnified bright field STEM-HAADF image, enclosed by red box in Fig. 5b, also more visible recrystallized grains. The EDX line scan

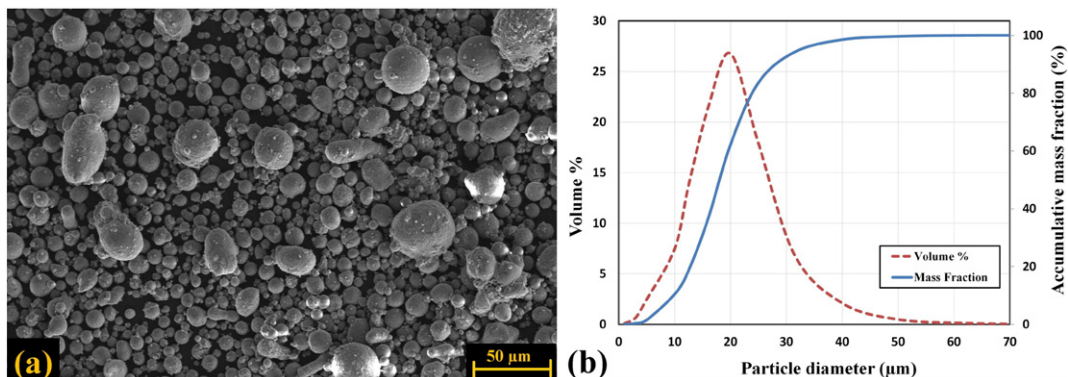


Fig. 2. a) SEM image of Al7075 powder; b) particle size distribution for Al7075.

Table 2

Cold spray coating parameters [9].

Carrier gas	Gas temperature	Gas pressure	Powder feed rate	Nozzle speed	Step over	Stand-off distance	Nozzle type	Nozzle length	Nozzle orifice diameter	Nozzle exit diameter
N ₂	400 °C	200 Psi (1.38 MPa)	8 g/min (5 rpm)	2 mm/s	1.2 mm	12 mm	De Laval UltiLife TM	120 mm	2 mm	6.3 mm

confirms the mixture of Al and Mg elements with Zn. The microstructure of the coating of Al7075 alloy shows elongated grains with ladder-like morphology. The grain refinement and diffusion of Al in Mg were the effect of impact temperature. The induced high impact and severe plastic deformation at higher strain rate causes the dynamic recrystallization of Mg, which enhances the refinement of grains, resulting in nano grains at the interface.

3.3. Microstructure of the substrate

To study the effects of carrier gas temperature and carrier gas temperature exposure time on the microstructure of AZ31B-H24 substrate samples, grain structure evaluations of sample cross-sections were conducted before and after coating deposition. For the sake of comparison, the cold-spray coating experiments were conducted with different nozzle velocities ($V = 2 \text{ mm/s}$ and $V = 10 \text{ mm/s}$). Low and high magnification microstructure images of the as-received samples are shown in Fig. 6a and b. These images reveal that the microstructure of the sample close to the surface was uniform, and no significant differences are observable on the surface or in the bulk close to the surface. After the cold spray coating, in the sample with high nozzle velocity ($V = 10 \text{ mm/s}$), the grain size of the Mg near the interface was decreased, as clearly seen in the low and high magnification SEM images of the cross-section (Fig. 6c and d). It is well known that plastic

deformation of a crystalline material increases the densities of crystal lattice defects, particularly resulting in dislocations. An accumulation of dislocations in the deformed grains leads to local misorientation in the grains that increases the energy of the crystal; hence, the dislocations will align inside of the grain and make sub-grain boundaries to reduce this excess energy. Further deformation of these grains would produce more rotation in the sub-grains, forming high angle grain boundaries and dividing the grains into smaller individual grains [45]. Based on this explanation, greater deformation should result in smaller grains. To evaluate this hypothesis, another coating was done with low nozzle velocity ($V = 2 \text{ mm/s}$). This would result in more peening time and hence more deformation in the substrate was expected. However, as seen in Fig. 6e and f, the grain size of the substrate at the interface is larger than the former case ($V = 10 \text{ mm/s}$). This can be attributed to the grain growth during the latter process. Decreasing the nozzle travel speed not only increased the peening time by 80%, but also exposed more heat to the substrate over a longer period of time as the coating process time took longer and hot gas flow exposure to the substrate increased. Therefore, beside the grain refinement due to the peening effect, the excessive heat associated with longer exposure time facilitated grain growth. While, grain refinement was still observable when the coated samples with lower nozzle velocity were compared to as-received samples, grain growth due to higher heat resulted in larger grain sizes when compared to the coating with higher

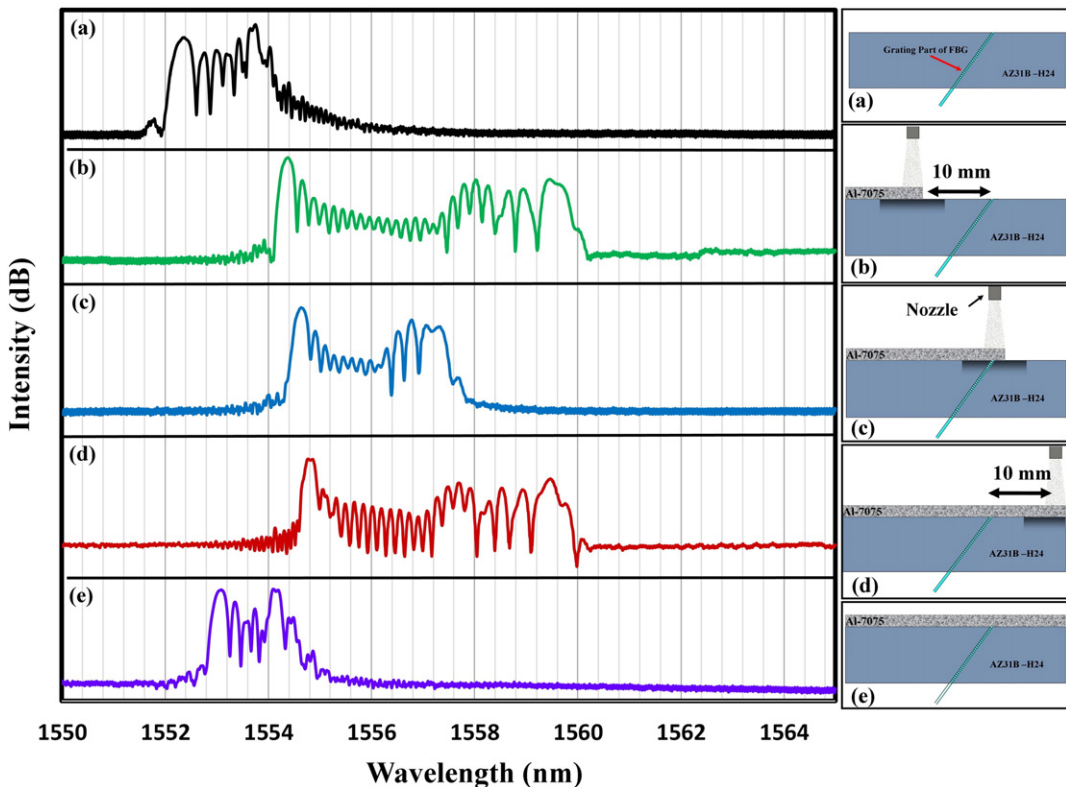


Fig. 3. Schematic of the coating process (right) and spectrum of FBG sensor response (left): a) after embedding the sensor and before the coating process; b) during coating at a location 10 mm away from the sensor; c) coating on the sensor; d) at 10 mm away from the sensor; e) after coating and substrate reach room temperature.

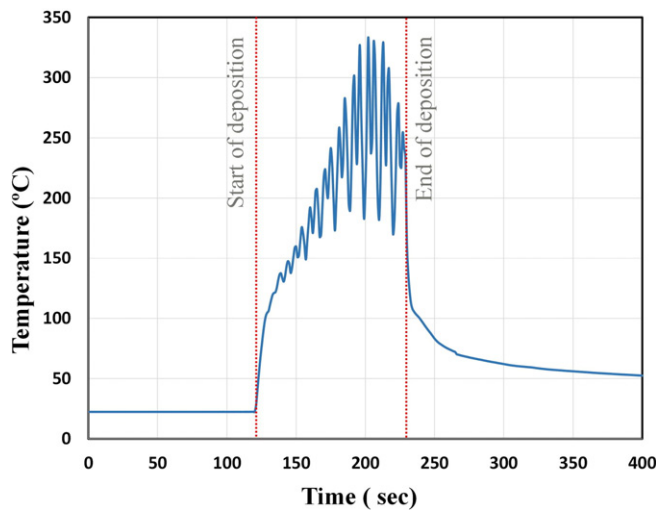


Fig. 4. Temperature of substrate measured by thermocouple during coating process.

nozzle velocity. To compare the microstructure evolution in the samples, the grain size of each sample was measured at the interface to 30 μm below the surface (Fig. 7). Based on this measurement, the average grain size of the as-received sample was 3.2 μm . For the cold spray with high nozzle travel speed ($V = 10 \text{ mm/s}$), the minimum grain size was not only 60% smaller than that seen after cold spraying at low nozzle travel speed (2 mm/s), but the effect of peening was observable in deeper areas (Fig. 7).

To eliminate the effects of carrier gas temperature on the substrate, the coating was done at room temperature with two different gas

pressures: $P = 96 \text{ Psi}$ (0.66 MPa) and $P = 200 \text{ Psi}$ (1.38 MPa). The surface was peened by Al particles; however, no deposition occurred. Fig. 8a and b illustrates the microstructure of the substrate after peening at $P = 96 \text{ Psi}$ at room temperature. These images clearly show grain refinement near the substrate's surface when compared to the coated samples shown in Fig. 6c to f. Fig. 8c and d demonstrates that increasing the gas pressure to 200 Psi dramatically reduced the grain size of the substrate surface beyond that of the sample coated at $P = 96 \text{ Psi}$, while the grains below the surface layer were deformed to lamellar grains. By comparing the peened samples (Fig. 8) and coated samples (Fig. 6) it would be hypothesized that the temperature of the cold spray was high enough to not only relax the induced residual stress during cold spraying but to allow grain growth. Microstructure observations reveal that the peening of the magnesium AZ31B-H24 substrate by Al7075 powder, in the condition of experiments, has enough energy to aggressively deform the grains near the substrate surface and lead to dynamic recrystallization and grain refinement. However, the average grain size of substrate near the surface for the peened samples is smaller than the coated samples. In cold spray, two sources of thermal energy are available: 1) thermal energy from the hot carrier gas and 2) thermal energy of the local plastic deformation due to high impact of particles with substrate. While the severe plasticity due local deformation of particle and substrate and released heat upon impact results in grain refinement near surface, the exposure of carrier gas over the deformed zone after collision lead to grain growth which results in larger grain in coated samples as compared to only-peened samples.

3.4. Residual stress measurement

The influence of relevant cold spray parameters on inducing compressive residual stress in Mg alloy substrate samples was further

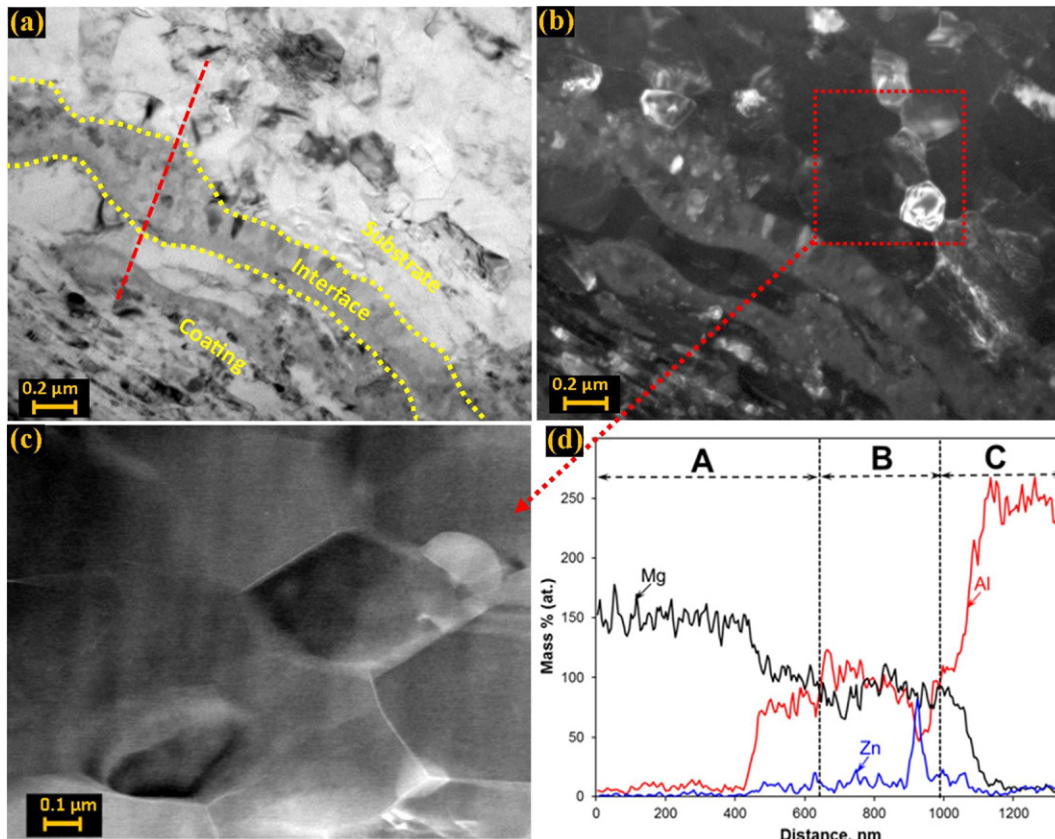


Fig. 5. Typical TEM micrograph lines show the microstructure at different zones: substrate (A), interface (B) and coating (C) of AZ31B alloy coated with Al7075 alloy in different modes, (a) bright field image, (b) dark field image, (c) STEM-High-angle annular dark-field (HAADF) image and (d) EDX line scan.

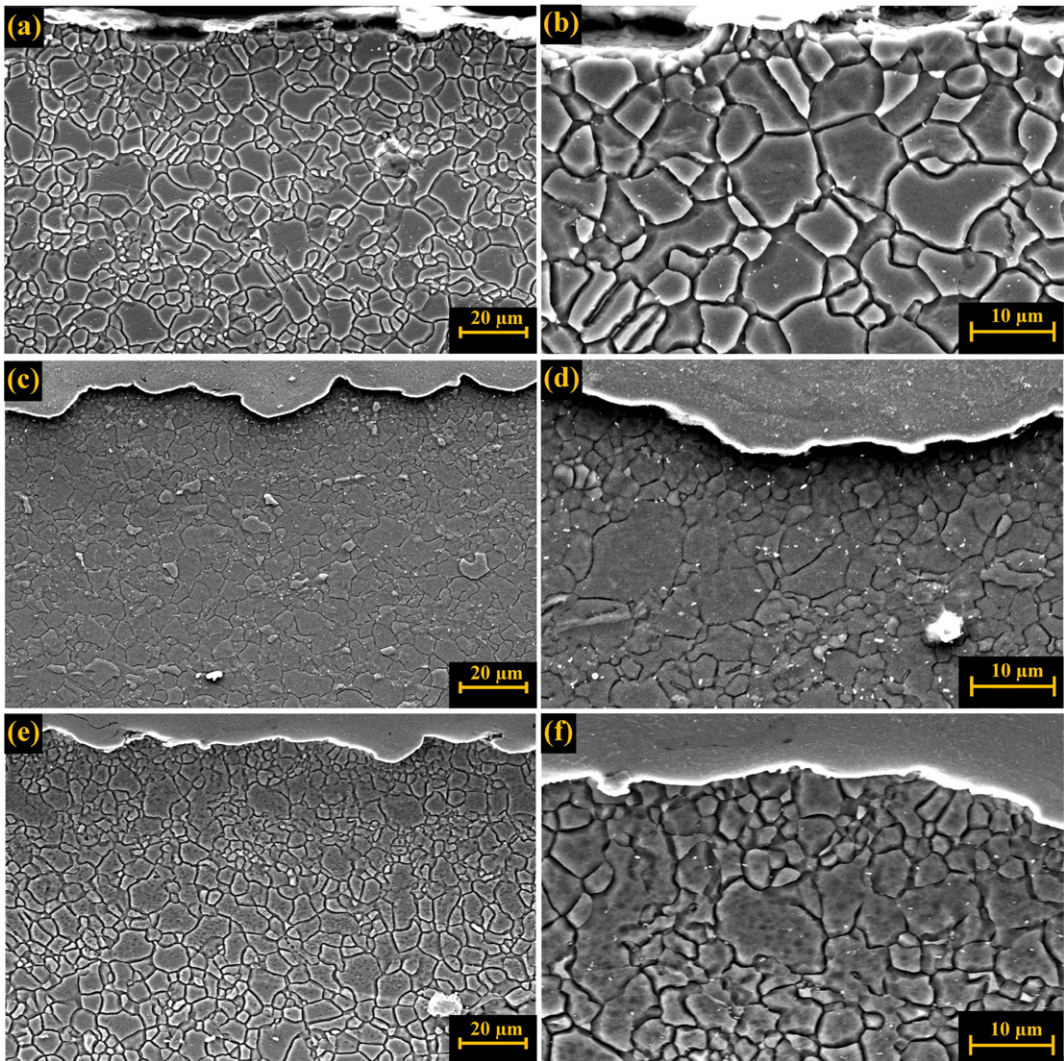


Fig. 6. a) and b) low and high magnification SEM images of the as-received sample; c) and d) low and high magnification SEM images of the sample after cold-spray coating ($V = 10 \text{ mm/s}$); e) and f) low and high magnification SEM images of the sample after cold-spray coating ($V = 2 \text{ mm/s}$).

investigated by conducting individual experiments and measuring the residual stress. The processing parameters used in the four experiments are listed in [Table 3](#). First the cold spray test was carried out without

spraying Al7075 powder, while the gas temperature and pressure were 400°C and 200 Psi, respectively (sample 1). The residual stress measurements were conducted using the hole-drilling method. [Fig. 9a](#) shows the stress profile of the Mg alloy substrate sample before and after the test. The stress measurements illustrate that the compressive residual stress decreased 83% near the substrate surface due to temperature effects. As the test was done without powder no deposition occurred, hence, the results were not affected by rising localized temperature due to impact. In sample 2, the effect of nozzle temperature was controlled with conducting the test at room temperature, imposing the peening process. In this condition, the cold spray test was conducted with 200 Psi pressure of flow gas with a powder feed rate of 8 g/min. Examination of the sample revealed that the peening effect increased 27% the compressive residual stress of the substrate ([Fig. 9b](#)) as expected from the microstructure evolution findings of the peened sample. By increasing the carrier gas temperature to create a relatively high quality of coating in sample 3, not only was the stress of the Mg alloy substrate relieved, but the stress was also released near the surface of the Al coating ([Fig. 9c](#)). Finally, the influence of sample carrier gas temperature exposure time on the residual stress was studied by increasing the velocity of the nozzle to 10 mm/s in sample 4 (i.e., decreasing the exposure time). The stress relaxation measurement demonstrated that increasing the nozzle travelling speed during the coating of the sample did not provide high enough thermal energy

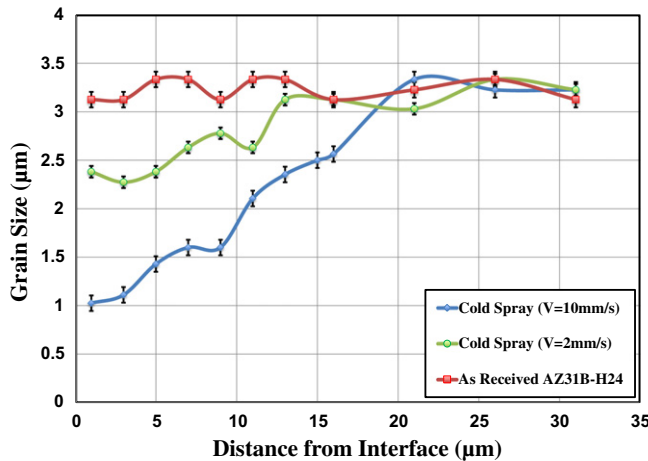


Fig. 7. Changes in grain size for three samples adjacent to the interface: as received, coated with low nozzle velocity, and coated with high nozzle velocity.

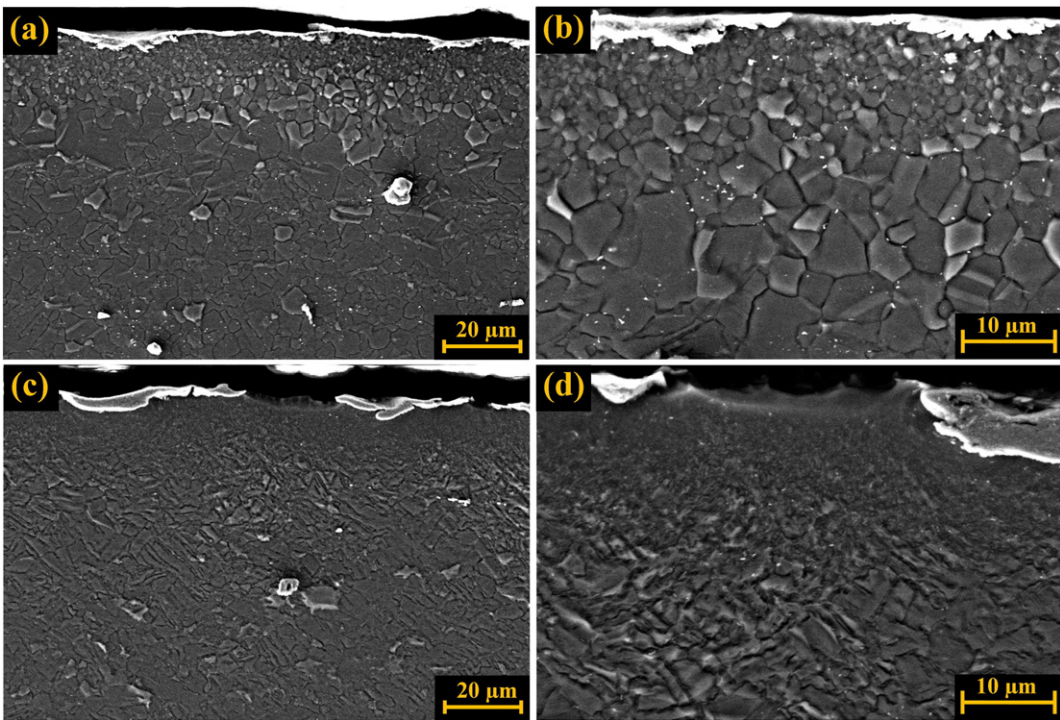


Fig. 8. Microstructure of the peened sample by aluminum particles, a) and b) $P = 96$ Psi at low and high magnifications SEM; c) and d) $P = 200$ Psi at low and high magnifications SEM images.

to relieve the residual stress of the Al coating, but the time was sufficient to release the residual stress of the Mg alloy substrate (Fig. 9d). Based on these observations, inducing residual stress in Mg substrate is a function of several variables.

By comparing the residual stress change variations across samples 1 to 4 following observations are made: 1) the heat transfer from 400 °C carrier gas to the Mg alloy substrate was not able to provide enough thermal energy to completely relieve the stresses of the Mg alloy substrates; 2) the peening process was able to induce high level of residual stress in the Mg alloy substrates; 3) the thermal energy released during adiabatic shear deformation due to Al7075 deposition, in addition to the thermal energy from the carrier gas, provided sufficient energy to anneal the Mg alloy substrates (compatible with the microstructural observations made above); and 4) the travelling speed of the nozzle was an important parameter that could affect the residual stress of the Al7075 coating while not affecting the residual stress of Mg alloy substrate (as far as the current examination extended).

3.5. Design of experiment

The design of experiments method was employed to evaluate the contribution of significant processing factors on the substrate's residual stress [46]. This design had three factors (2^3 full factorial): pressure of

carrier gas, temperature of carrier gas, and velocity of the nozzle. All three factors play considerable role in successful coating. The pressure of carrier gas provides the kinetic energy to the particles needed for high impact collision. The temperature of carrier gas generates thermal energy for the particles to have the required ductility for successful deposition on the substrate. The nozzle velocity influences the thickness of the coating and the exposure time to carrier gas temperature. Each of these factors had two levels of high and low. Based on the full factorial design, eight trials were planned. The responses for each trial included residual stress measurements were repeated at three different points on each sample, before and after applying the cold-spray process. Hence, a total of 48 residual stress measurements were made under different conditions. STATISTICA software was employed to analyze the results with a confidence level of 95%. Since only residual stresses at the surface were of interest, all of the residual stress measurements were conducted using the X-ray diffraction method.

First, the low level of gas pressure was determined with respect to the coating deposition condition. For this purpose, the cold-spray coating process was done for different levels of pressure while the temperature of gas flow was kept at 400 °C. The substrate weight was measured before and after the coating process, for each gas pressure. The weight change of the substrate samples versus pressure is shown in Fig. 10. As the pressure increased, up to a pressure of 92 Psi, the weight of substrate decreased due to the abrasion of the substrate. At around 96 Psi, the sample weight change was essentially zero and above that weight was added to the substrate indicating successful coating. Based on this observation, it was considered that coating deposition occurred after the critical value of 96 Psi of pressure was reached.

The microstructure of a sample coated at a pressure of 100 Psi, and a map of the alloying distribution are shown in Fig. 11a and b. The SEM results revealed that 64% of the sample was coated by Al7075 powder at a pressure of 100 Psi, confirming that Al particles were deposited onto the Mg substrate at pressures above 96 Psi.

Based on the experimental design, four experiments were performed at low carrier gas temperatures (room temperature) with two

Table 3
Cold spray parameters for hole-drilling measurements.

Sample number	Gas pressure (Psi)	Gas temperature (°C)	Nozzle speed (mm/s)	Powder feed rate (g/min)
1	200	400	2	0
2	200	23	2	8
3	200	400	2	8
4	200	400	10	8

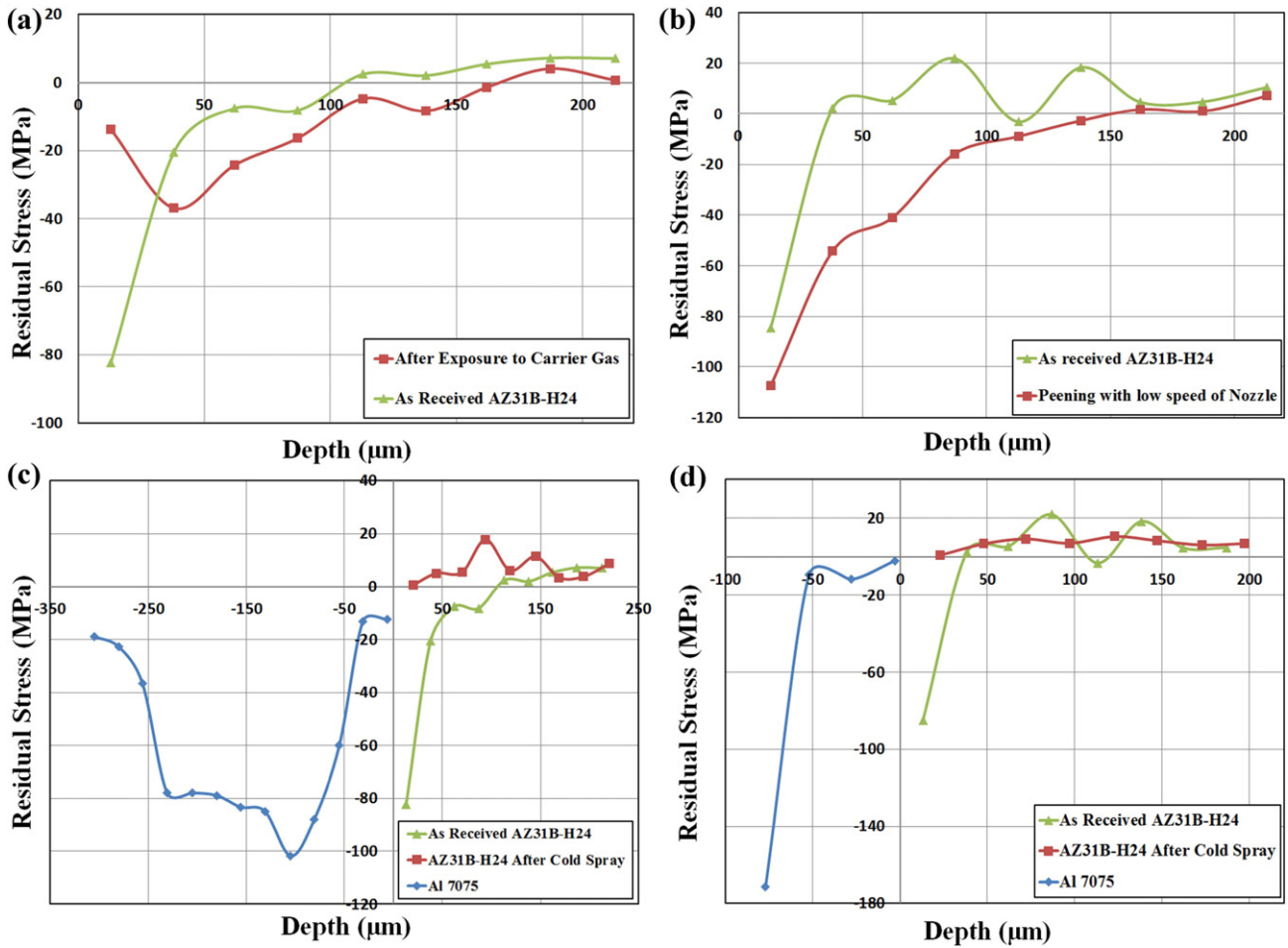


Fig. 9. Residual stress measurement by hole drilling: a) cold spray without spraying powder (exposure to carrier gas); b) cold spray at room temperature (peening effect); c) cold spray test ($V = 2 \text{ mm/s}$); d) cold spray test ($V = 10 \text{ mm/s}$).

different levels of gas pressure and nozzle speed. Al alloy powder impinged the substrate with high speed and produced dimples on the surface. At room temperature, coating deposition did not occur; however, the role of the peening process in increasing the compressive residual stress could be highlighted. Fig. 12a shows the average measurement of residual stress for AZ31B-H24 samples before and after cold-spray coating tests. The green bars represent the average residual stress measurements for as-received samples before conducting the experiment, and the brown bars specify the residual stress values obtained after cold-spray tests were conducted under the different processing parameters. The differences between the initial induced residual stresses of as-received AZ31B-H24 samples and the generated residual stresses after cold-spray tests are presented in Fig. 12b. The results reveal that cold-spray processing at a low temperature of carrier gas increases the compressive residual stress, irrespective of the gas pressure value or nozzle speed level. However, as the carrier gas temperature increased, the results were completely dependent on the gas pressure and nozzle speed. In this situation, at low gas pressure, the compressive residual stress was reduced in the specimen surface when the nozzle speed was 2 mm/s. Since increasing the nozzle speed decreases the exposure time of the Mg substrate during which it can obtain energy from the carrier gas temperature, the reduction in compressive residual stress was negligible with a nozzle speed of 10 mm/s (see Fig. 12a–b). In contrast, increased gas pressure in conjunction with high gas temperature boosted the kinetic energy of the particles. During impact, the kinetic energy is transformed to internal energy in the particles and substrate

surface grains. This phenomenon happens over a very short impact time; hence, there is not enough time for the heat to transfer to the substrate and environment. The localized temperature generated at the interface increases dramatically, leading to softening of the crystalline

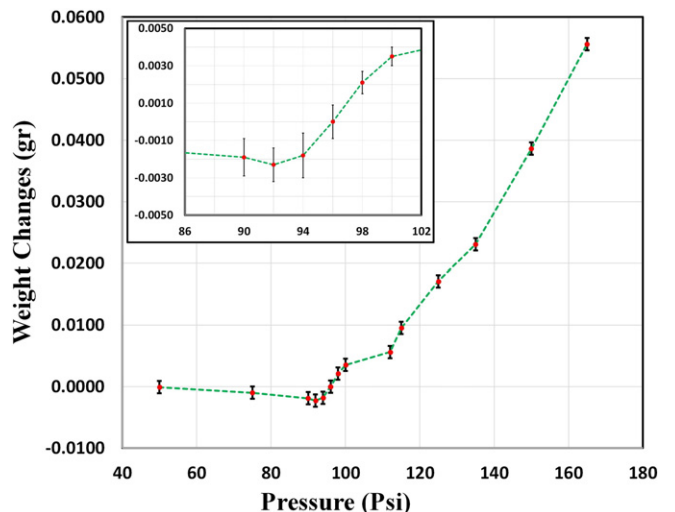


Fig. 10. Change in the weight of substrate at different pressures.

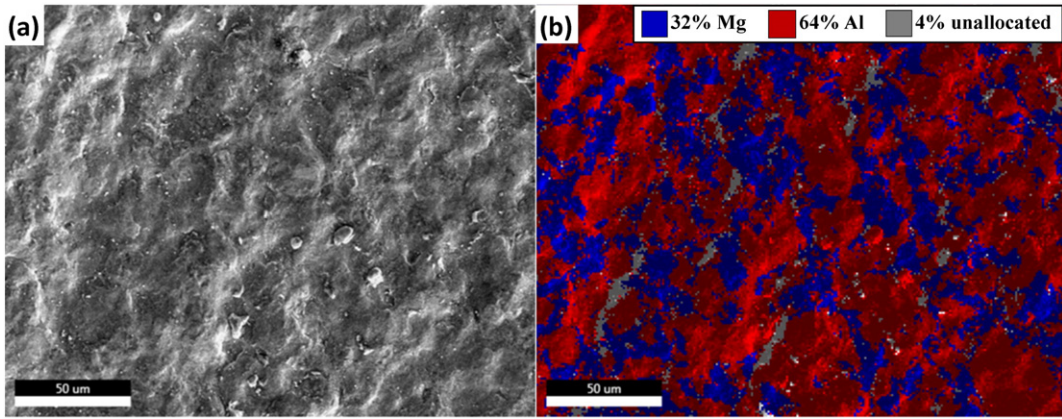


Fig. 11. a) Surface of coated sample and b) map of alloying distribution at pressure of 100 Psi.

material. Rising temperature allows the particles and substrate surface grains to deform and enables metallurgical bonding at the interface. The mechanism of coating deposition, adiabatic shear instability, along with carrier gas temperature provides enough energy to release the compressive residual stress of the substrate. The results obtained at high gas pressure and temperature demonstrate that the residual stresses of the samples are completely released and the original compressive residual stresses of the as-received samples are replaced by tensile stresses (Fig. 12a–b). This observation is compatible with the in situ observation data gathered by the embedded FBG sensor. However, based on the progressive coating deposition model and corresponding literature, residual stresses are strongly related to kinetic energy rather than thermal effects in copper/Al coated samples. Also, it has been claimed that the effects of thermal mismatch on stress relaxation have been neglected, and that these could be extended to all coating materials and substrate selections [19].

To recognize the effects of significant factors on the substrate residual stress changes, an analysis of response variance was made using ANOVA (Table 4) [46]. The results demonstrate that there exist statistically significant relationships between the sources of variation and the residual stress change responses. Indeed, the results reveal that the temperature and pressure of carrier gas have more significant effects than other variables, although all of the identified factors are strongly related to the residual stress response (p -value < 0.05). Furthermore, based on the coefficients of determination squared R (0.989) and

adjusted R^2 (0.984) were calculated by Eqs. (5) and (6). As these values are both very close to one, it is clear that the regression line model almost perfectly fits the data.

$$R^2 = \frac{SSR}{SST} \quad (5)$$

$$R_{Adj}^2 = 1 - \left[\frac{(1-R^2)(n-1)}{n-q-1} \right] \quad (6)$$

where SSR (sum of squares regression) is the sum of the squared differences between the prediction for each observation and the population mean, which is equal to SST-SSE. In Eq. (6), n is the number of observations, 24, and $q=7$ is the number of significant parameters, considering the error.

To further confirm that the data fit the model reasonably well, the residual plots (the most valuable regression diagnostic tools) were extracted (see Fig. 13). Residual terms refer to the difference between the observed value of the dependent variable and the predicted value of the regression analysis. Based on the residual plots obtained, the relationships between the dependent variable (residual stress change) and independent variables (gas temperature, gas pressure and nozzle speed) were linear, and the residual was distributed normally around the predicted dependent variables (Fig. 13a). Moreover, Fig. 13b

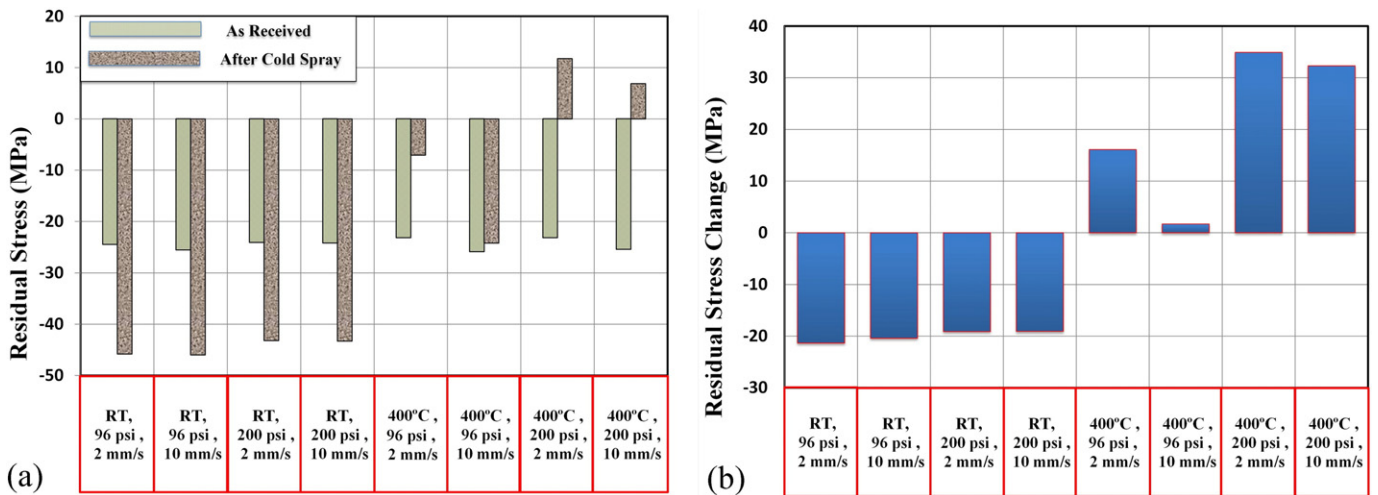


Fig. 12. Residual stress measurement by X-ray diffraction: a) for Mg AZ31B-H24 substrate before and after different processing parameters of cold-spray coating; b) difference between residual stresses of as-received substrate and substrate after different conditions of coating.

Table 4
ANOVA results.

Source of variation	Sum of squares (SS)	Degree of freedom	Mean squares	F ratio	p-Value
Temperature of carrier gas	10,201.45	1	10,201.45	1385.374	0.000000
Pressure of carrier gas	1054.60	1	1054.60	143.216	0.000000
Speed of the nozzle	96.42	1	96.42	13.095	0.002121
Temperature * pressure	790.14	1	790.14	107.303	0.000000
Temperature * speed	121.20	1	121.20	16.460	0.000819
Pressure * speed	44.81	1	44.81	6.085	0.024556
Error	125.18 (SSE)	17			
Total SS	12,433.81 (SST)	23			

shows that the data was statistically independent, because the magnitudes of the residuals were completely random. The independent variables had almost equal variance around the regression line, meaning that the variance is a deviation from the best-fit line. Therefore, this model had enough validity to be used to predict the change of residual stress in the substrate in relation to the identified significant processing parameters. However, based on observations made from two random combination tests, the regression equation could behave non-linearly, especially around the area where coating occurs. The following predictive stress relaxation equation was obtained from the linear regression analysis of the identified processing parameters:

$$\text{Residual Stress Change} = -17.98 + 0.0406T - 0.0357P - 0.8430V + 0.0006TP - 0.003TV + 0.0066PV \quad (7)$$

Using the generated statistical model, three-dimensional (3D) fitted surface plots were created to explore the relationships between the significant processing parameters of cold-spray coating and residual stress variation in the Mg alloy substrate samples. Fig. 14 indicates the relationship between two independent parameters, carrier gas pressure and nozzle velocity, and the residual stress variation, at two different levels of temperature. According to the obtained surface plots, the parameter having the biggest effect on residual stress change is carrier gas temperature, as it has the biggest variation domain (-23°C to 40°C). This is compatible with the ANOVA results. At room temperature, a high compressive residual stress change (less than -23 MPa) is observed in the conditions of high gas pressure and low speed of nozzle (Fig. 14a). At high gas pressure and high speed of nozzle, a significant compressive residual stress change (more than -17 MPa) was

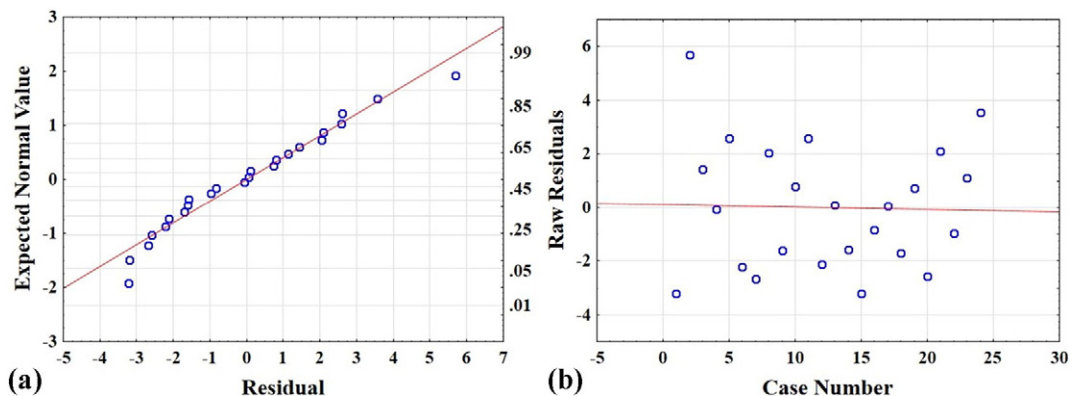


Fig. 13. a) Normal probability plot; b) selected raw residual values against the case numbers for each case or run.

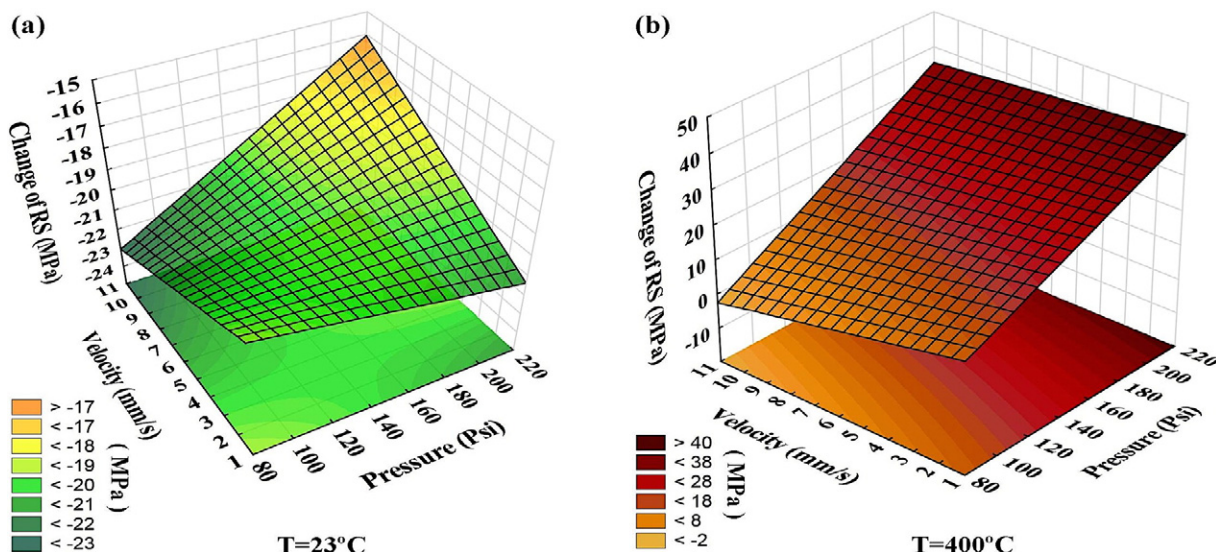
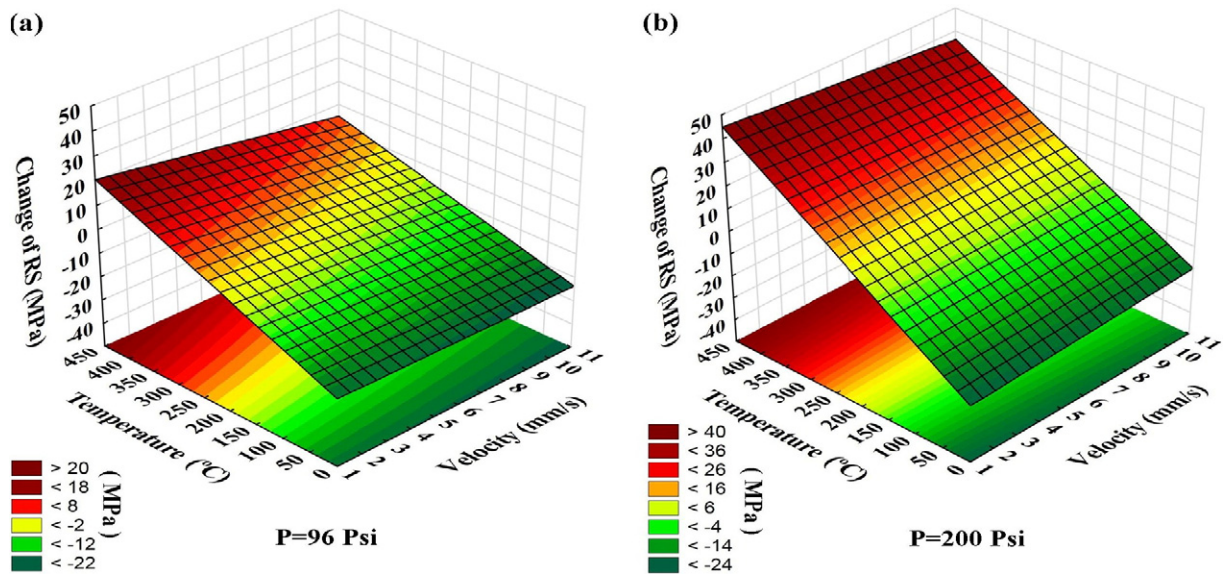


Fig. 14. 3D surface plot at a) $T = 23^{\circ}\text{C}$ and b) $T = 400^{\circ}\text{C}$.

Fig. 15. 3D surface plot at a) $P = 96$ Psi and b) $P = 200$ Psi.

achievable (Fig. 14a); however, no deposition occurred at room temperature. After increasing the carrier gas temperature to $400\text{ }^{\circ}\text{C}$, the change varied between -2 MPa and 40 MPa , corresponding to low gas pressure and high nozzle speed, and high gas pressure and low nozzle speed, respectively (see Fig. 14b). This range of residual stress variation is not sufficient to improve fatigue life. It is of note that at a high carrier gas temperature, increasing the nozzle speed does not significantly improve the compressive residual stress in the substrate, nor does decreasing the gas pressure. However, at a low gas pressure, increasing the nozzle speed helped to boost the compressive residual stress in the substrate.

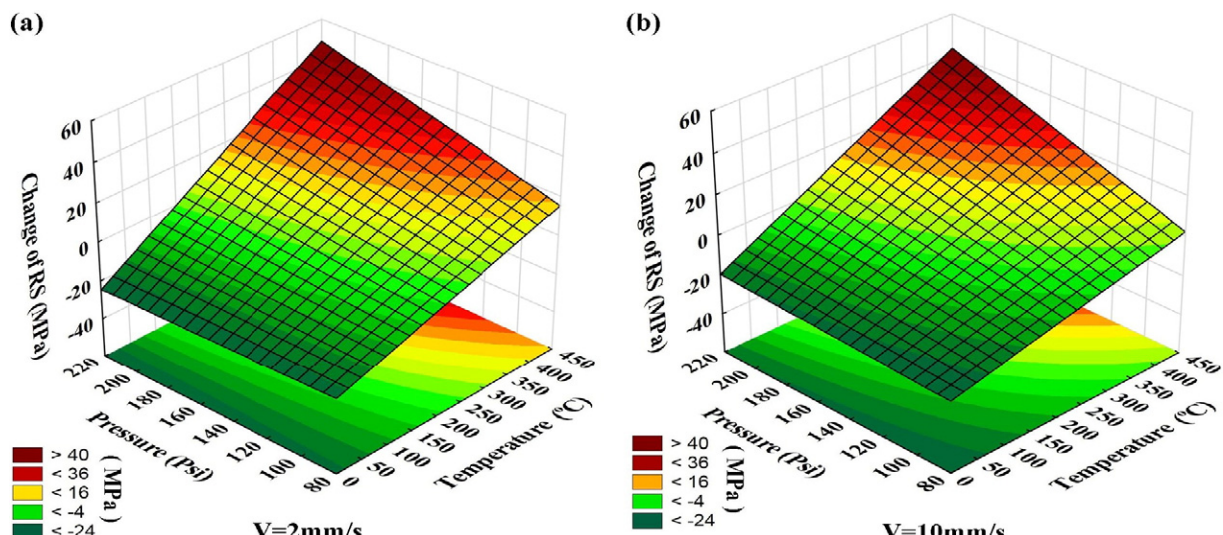
The variety of residual stress changes can be predicted with a 3D surface plot when the carrier gas pressure was kept constant at low and high levels (see Fig. 15). At both levels of pressure, 96 Psi and 200 Psi, when the carrier gas temperature is below $150\text{ }^{\circ}\text{C}$, the maximum changes of compressive residual stress can be predicted at any level of nozzle speed. However, at high carrier gas pressure, a greater slope of response surface can be observed, which includes a bigger domain of residual stress changes in the substrate while compared with the low carrier gas pressure results. In this situation, the effect of nozzle speed is not significant at low temperature at either level of pressure. The effect of

nozzle speed is specified in Fig. 16. Based on the prediction model, the ranges of residual stress variation at low and high levels of nozzle speed are the same, although increasing the nozzle speed can lead to better predictions of compressive residual stress changes at higher temperatures. Employing the results of this research to induce maximum possible residual stress along with grain refinement of the substrate toward enhancing fatigue performance of magnesium alloy will be examined in future.

4. Conclusions

The effect of cold-spray deposition processing parameters on the residual stress induced in Mg alloy substrates was investigated. Thermo-mechanical strain evolution and interaction effects were monitored in situ through embedded FBG sensors under the optimum cold-spray coating condition. The following conclusions can be drawn from the results obtained in this study:

- 1) The embedded FBG sensors were able to monitor the thermo-mechanical strain evolution of samples during the cold-spray coating

Fig. 16. 3D surface plot at a) $V = 2\text{ mm/s}$ and b) $V = 10\text{ mm/s}$.

- process. The in situ observations uncovered that the compressive strain created in the substrate during cold-spray coating was released after a few seconds. Thermocouple data recorded during coating revealed that the substrate was warmed up to 330 °C for a short period.
- 2) The substrate grain size was found to be a function of the absorbed thermal energy; more transferred heat to the substrate led to larger grains.
 - 3) The consistency of the results obtained from in situ strain and temperature measurements during coating, microstructural changes of the sample and residual stress measurements lead to the conclusion that the high energy generated by Al particles during the peening process led to grain refinement of the substrate surface and induced higher compressive residual stress in the sample. However, the temperature of the cold gas spray was sufficient for the AZ31B Mg sample to not only recover the residual stress of the substrate but also provide enough energy for recrystallization and partial grain growth in the substrate close to the interface.
 - 4) Based on the statistical analysis, the temperature and pressure of the carrier gas had the most significant impact on the residual stress variation of the examined parameters; and, the interaction of the carrier gas pressure and the speed of nozzle had minimal effect.

Acknowledgements

The financial support of the Natural Sciences and Engineering Research Council of Canada (NSERC) through the Automotive Partnership Canada (APC) under APCPJ 459269–13 grant with contributions from Multimatic Technical Centre, Ford Motor Company, and Centerline Windsor are acknowledged. Funds from NSERC-RTI program under EQPEQ 458441-2014 grant also supported this research. The authors would also like to thank Dr. R. Ghelichi for discussions, and Dr. S.K. Shaha for the TEM images.

References

- [1] R.I. Stephens, A. Fatemi, R.R. Stephens, H.O. Fuchs, Metal Fatigue in Engineering, 2nd ed. Wiley, 2000.
- [2] A.H. Mahmoudi, A. Ghasemi, G.H. Farrahi, K. Sherafatnia, A comprehensive experimental and numerical study on redistribution of residual stresses by shot peening, *Mater. Des.* 90 (2016) 478–487.
- [3] S.M. Hassani-Gangaraj, M. Carboni, M. Guagliano, Finite element approach toward an advanced understanding of deep rolling induced residual stresses, and an application to railway axles, *Mater. Des.* 83 (2015) 689–703.
- [4] H. Jahed, R. Ghelichi, Residual stresses and fatigue life enhancement of cold spray, in: J. Villafuerte (Ed.), Modern Cold Spray: Materials, Process, and Applications, Springer International Publishing, Cham 2015, pp. 225–252.
- [5] R.N. Raefelson, C. Verdy, H. Liao, Cold gas dynamic spray additive manufacturing today: deposit possibilities, technological solutions and viable applications, *Mater. Des.* 133 (2017) 266–287.
- [6] J. Villafuerte, Modern Cold Spray:Materials, Process, and Applications, Springer International Publishing, 2015.
- [7] H. Assadi, F. Gärtner, T. Stoltenhoff, H. Kreye, Bonding mechanism in cold gas spraying, *Acta Mater.* 51 (15) (2003) 4379–4394.
- [8] R. Ghelichi, D. MacDonald, S. Bagherifard, H. Jahed, M. Guagliano, B. Jodoin, Microstructure and fatigue behavior of cold spray coated Al5052, *Acta Mater.* 60 (19) (2012) 6555–6561.
- [9] S. Dayani, R. Ghelichi, S. Shaha, J. Wang, H. Jahed, The impact of Al7075 cold spray coating on the fatigue life of AZ31B cast alloy, *Surf. Coat. Technol.* (June 2017) (Submitted (Under Review)).
- [10] P. Cavaliere, A. Silvello, Processing conditions affecting residual stresses and fatigue properties of cold spray deposits, *Int. J. Adv. Manuf. Technol.* 81 (9–12) (2015) 1857–1862.
- [11] T.S. Price, P.H. Shipway, D.G. McCartney, Effect of cold spray deposition of a titanium coating on fatigue behavior of a titanium alloy, *J. Therm. Spray Technol.* 15 (4) (2006) 507–512.
- [12] J. Cizek, O. Kovarik, J. Siegl, K.A. Khor, I. Dilouhy, Influence of plasma and cold spray deposited Ti layers on high-cycle fatigue properties of Ti6Al4V substrates, *Surf. Coat. Technol.* 217 (2013) 23–33.
- [13] X. Yuming, Z. Ming-Xing, The effect of cold sprayed coatings on the mechanical properties of AZ91D magnesium alloys, *Surf. Coat. Technol.* 253 (2014) 89–95.
- [14] S. Yin, E.J. Ekoi, T.L. Lupton, D.P. Dowling, R. Lupoi, Cold spraying of WC-Co-Ni coatings using porous WC-17Co powders: formation mechanism, microstructure characterization and tribological performance, *Mater. Des.* 126 (2017) 305–313.
- [15] F. Meng, D. Hu, Y. Gao, S. Yue, J. Song, Cold-spray bonding mechanisms and deposition efficiency prediction for particle/substrate with distinct deformability, *Mater. Des.* 109 (2016) 503–510.
- [16] C.W. Zieman, M.M. Sharma, B.D. Bouffard, T. Nissley, T.J. Eden, Effect of substrate surface roughening and cold spray coating on the fatigue life of AA2024 specimens, *Mater. Des.* 54 (2014) 212–221.
- [17] A. Moridi, S.M. Hassani-Gangaraj, M. Guagliano, S. Vezzu, Effect of Cold Spray Deposition of Similar Material on Fatigue Behavior of Al 6082 Alloy, The Society for Experimental Mechanics, USA, 2013 51–57.
- [18] K. Spencer, V. Luzin, N. Matthews, M.X. Zhang, Residual stresses in cold spray Al coatings: the effect of alloying and of process parameters, *Surf. Coat. Technol.* 206 (19–20) (2012) 4249–4255.
- [19] V. Luzin, K. Spencer, M.X. Zhang, Residual stress and thermo-mechanical properties of cold spray metal coatings, *Acta Mater.* 59 (3) (2011) 1259–1270.
- [20] L. Wenyia, Y. Kang, Z. Dongdong, Z. Xianglin, G. Xueping, Interface behavior of particles upon impacting during cold spraying of Cu/Ni/Al mixture, *Mater. Des.* 95 (2016) 237–246.
- [21] F. Wang, M. Zhao, Simulation of particle deposition behavior in cold-sprayed Mg anticorrosion coating, *Mater. Manuf. Process.* 31 (11) (2014) 1483–1489.
- [22] A.N. Ryabinin, Calculation of the particle velocity in cold spray in the one-dimensional non-isentropic approach, *ARPENJ. Eng. Appl. Sci.* 10 (6) (2015) 2435–2439.
- [23] V.K. Champagne, D.J. Helfritch, M.D. Trexler, B.M. Gabriel, The effect of cold spray impact velocity on deposit hardness, *Model. Simul. Mater. Sci. Eng.* 18 (6) (2010) 065011.
- [24] G. Bae, Y. Xiong, S. Kumar, K. Kang, C. Lee, General aspects of interface bonding in kinetic sprayed coatings, *Acta Mater.* 56 (17) (2008) 4858–4868.
- [25] P. Cavaliere, A. Silvello, Fatigue behaviour of cold sprayed metals and alloys: critical review, *Surf. Eng.* 32 (9) (2016) 631–640.
- [26] S. Rech, A. Trentin, S. Vezzù, J.-G. Legoux, E. Irissou, M. Guagliano, Influence of pre-heated Al 6061 substrate temperature on the residual stresses of multipass Al coatings deposited by cold spray, *J. Therm. Spray Technol.* 20 (1–2) (2010) 243–251.
- [27] D. Lehnhus, A.V. Hehl, K. Kayvantash, R. Gradinger, T. Becker, K. Schimanski, M. Avalle, Taking a downward turn on the weight spiral – lightweight materials in transport applications, *Mater. Des.* 66 (2015) 385–389.
- [28] M. Gupta, N.M.L. Sharon, Magnesium, Magnesium Alloys, and Magnesium Composites, Wiley, 2011.
- [29] B.L. Mordike, T. Ebert, Magnesium: properties – applications – potential, *Mater. Sci. Eng. A* 302 (2001) 37–45.
- [30] S.D. Wang, D.K. Xu, B.J. Wang, E.H. Han, C. Dong, Effect of corrosion attack on the fatigue behavior of an as-cast Mg–7%Gd–5%Y–1%Nd–0.5%Zr alloy, *Mater. Des.* 84 (2015) 185–193.
- [31] G. Shayegan, H. Mahmoudi, R. Ghelichi, J. Villafuerte, J. Wang, M. Guagliano, H. Jahed, Residual stress induced by cold spray coating of magnesium AZ31B extrusion, *Mater. Des.* 60 (2014) 72–84.
- [32] ASM Handbook, ASM International, 1991.
- [33] M.M. Avedesian, H. Baker, ASM Specialty Handbook: Magnesium and Magnesium Alloys, ASM International, 1999.
- [34] M.M. Werneck, R.C.S.B. Allil, B.A. Ribeiro, F.V.B.d. Nazaré, A Guide to Fiber Bragg Grating Sensors, InTech, 2013.
- [35] J.M. Dockney, R. Tatam, Simultaneous independent temperature and strain measurement using in-fiber Bragg grating sensors, *Electron. Lett.* 32 (12) (1996).
- [36] B. Marzbanrad, H. Jahed, E. Toyserkani, On the sensitivity and repeatability of fiber Bragg grating sensors used in strain and material degradation measurement of magnesium alloys under cyclic loads, *Int. J. Adv. Manuf. Technol.* 86 (9–12) (2016) 3453–3461.
- [37] A. Feng, D. Chen, C. Li, X. Gu, Flat-cladding fiber Bragg grating sensors for large strain amplitude fatigue tests, *Sensors (Basel)* 10 (8) (2010) 7674–7680.
- [38] E. Kalatehmollaie, H. Mahmoodi-Asl, H. Jahed, An asymmetric elastic–plastic analysis of the load-controlled rotating bending test and its application in the fatigue life estimation of wrought magnesium AZ31B, *Int. J. Fatigue* 64 (2014) 33–41.
- [39] E. Technology (Ed.), EPO-TEK 353ND, 2014.
- [40] G.S. Schajer, Measurement of non-uniform residual stresses using the hole-drilling method. Part II—practical application of the integral method, *J. Eng. Mater. Technol.* 110 (1988) 344–349.
- [41] B.D. Cullity, S.R. Stock, Elements of X-ray Diffraction, Scholar's Choice Edition ed. Addison-Wesley P Inc., USA, 2015.
- [42] R. Kashyap, Fiber Bragg Gratings, Second Edition Elsevier, United States of America, 2010.
- [43] Z. Arabgol, H. Assadi, T. Schmidt, F. Gärtner, T. Klassen, Analysis of thermal history and residual stress in cold-sprayed coatings, *J. Therm. Spray Technol.* 23 (1–2) (2013) 84–90.
- [44] S. Housh, B. Mikucki, A. Stevenson, Properties of Magnesium Alloys, Properties and Selection: Nonferrous Alloys and Special-Purpose Materials, ASM International, 1992.
- [45] A. Mishra, B. Kad, F. Gregori, M. Meyers, Microstructural evolution in copper subjected to severe plastic deformation: experiments and analysis, *Acta Mater.* 55 (1) (2007) 13–28.
- [46] D.C. Montgomery, Design and Analysis of Experiments, 8th ed. John Wiley & Sons, Inc., 2012.